nature catalysis

Article

https://doi.org/10.1038/s41929-026-01480-4

# Palladium-catalysed asymmetric *anti*-Michael-type addition of α,β-unsaturated carboxylic acids with carboranes

Received: 18 November 2024

Accepted: 7 January 2026

Published online: 30 January 2026

Check for updates

Chao Lei[1,3], Wen Lu[1,3], Tingting Shen[1,3], Meng Huang[1], Yan-Xuan Wu[1], Donghui Wei[1] ✉, Yan-Na Ma[1] ✉ & Xuenian Chen[1,2] ✉

The catalytic asymmetric Michael addition of α,β-unsaturated carbonyl compounds is one of the most valuable methods for constructing the β-carbon chirality centre because of its atom economy and efficiency. However, the catalytic asymmetric reverse α-addition of a nucleophile to an α,β-unsaturated carbonyl compound is much less common. Here we realize a palladium-catalysed asymmetric α-carboranylation of α,β-unsaturated carboxylic acids via an inverse electron-demand nucleophilic addition. The reaction features good B(9)-site selectivity of *o*/*m*-carboranes, precise α-regioselectivity towards α,β-unsaturated carboxylic acids, wide functional group tolerance and excellent enantioselectivities. A detailed reaction mechanism is proposed based on experimental and computational results that elucidates the origin of the enantioselectivity and α-selectivity. This finding has a guiding significance for the catalytic asymmetric *anti*-Michael-type addition of α,β-unsaturated carbonyl compounds and provides a different avenue for synthesizing α-chiral carboxylic acids.

Icosahedral carboranes (that is, $C_2B_{10}H_{12}$), a class of representative boron clusters with three-dimensional aromaticity, have potential applications in material chemistry, organic synthesis and pharmaceuticals[1–13]. In particular, carborane derivatives are very attractive in medicinal chemistry because of their ability to form unusual dihydrogen bonds that can target hydrophobic binding sites in different bioreceptors when designing bioactive compounds[2] (Fig. 1a). In addition, carboranes are potential candidates for boron neutron capture therapy due to their high boron content[13]. Consequently, developing new methods to introduce carboranes into organic molecules is highly desirable. Over the past several decades, various cage-carbon-substituted *o*-carborane derivatives were synthesized via reactions of decaborane with alkynes or cage C–H functionalization[14,15]. However, cage-boron-substituted *o*-carborane derivatives are less known due to the weak polarity of B–H bonds and the low selectivity of ten B–H bonds in *o*/*m*-carboranes. Notably, the B-substituted carborane cage behaves as an electron-rich moiety, in contrast to the C-substituted carborane cage as electron-withdrawing, making the derivatives show different properties[16]. Therefore, the selective B–H functionalization to access cage-boron-substituted *o*-carborane derivatives is of great significance, and some pioneering work has been reported in the last decade[17–23]. Despite these, the catalytic asymmetric synthesis to connect the boron vertex with the chiral carbon centre was not reported[24–26]. Using 1,1,1,3,3,3-hexafluoro-2-propanol (HFIP) as a solvent, our group realized a series of electrophilic substitution reactions on the B(9) position of *o*-carborane[27–30] (Fig. 1b). The Pd(II)-catalysed B(9)–H functionalization has also been developed via an electrophilic palladation process[31]. In these reactions, the carborane acts as a nucleophile to react with diverse electrophiles.

Catalytic asymmetric Michael addition is one of the most valuable methods for constructing β-chirality centre of α,β-unsaturated carbonyl compounds regarding their atom economy and green credentials (Fig. 1c). Therefore, a large variety of nucleophiles (Michael donors) and α,β-unsaturated compounds (Michael acceptors) have been employed in these reactions[32–41]. By contrast, catalytic

[1]College of Chemistry, Zhengzhou University, Zhengzhou, China. [2]School of Chemistry and Chemical Engineering, Henan Key Laboratory of Boron Chemistry and Advanced Materials, Henan Normal University, Xinxiang, China. [3]These authors contributed equally: Chao Lei, Wen Lu, Tingting Shen. ✉e-mail: donghuiwei@zzu.edu.cn; mayanna@zzu.edu.cn; xuenian_chen@zzu.edu.cn

https://doi.org/10.1038/s41929-026-01480-4

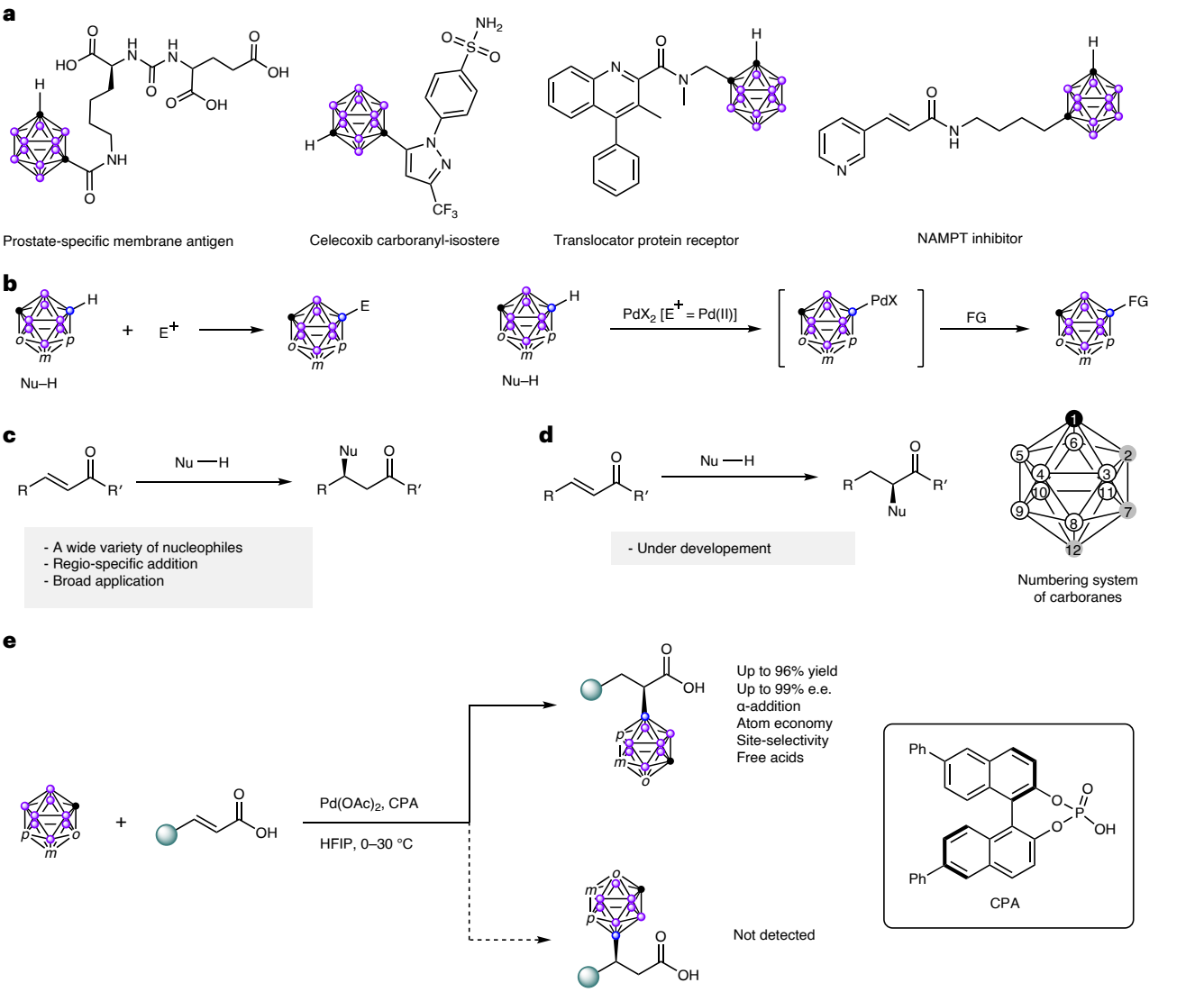


**Fig. 1 | Applications of carboranes and catalytic asymmetric Michael and *anti*-Michael addition. a**, Applications of carboranes in drug discovery and chemical biology. **b**, Electrophilic substitution reactions and Pd(II)-catalysed selective B–H activation of carboranes. **c**, Asymmetric Mechael addition reactions. **d**, Asymmetric anti-Mechael-type addition reactions. **e**, This work: Pd(II)-catalysed asymmetric Michael and *anti*-Michael addition of carboranes to α,β-unsaturated carboxylic acids. NAMPT, nicotinamide phosphoribosyltransferase; FG, functional group; α-addition, which refers to an addition reaction that occurs at the α-position of a carboxyl group.

asymmetric *anti*-Michael addition for constructing α-chiral centres of α,β-unsaturated carbonyl compounds has rarely been reported[42] (Fig. 1d). Nevertheless, given the significant importance of α-chiral carbonyl compounds in biologically active molecules and pharmaceuticals, the development of catalytic asymmetric *anti*-Michael additions remains highly appealing[43–45]. We wonder whether the carboranes can act as one kind of Michael donor to react with α,β-unsaturated carbonyl compounds. However, the low nucleophilicity of carboranes makes the directly nucleophilic addition impossible. Recently, we conducted a systematic investigation into the electrophilic substitution reactions of *o*-carborane and benzene. The results revealed that the hard electrophiles tend to react with benzene, whereas soft electrophiles exhibit a clear preference for *o*-carborane. This observation aligns perfectly with the hard and soft, acids and bases principle[30]. As a soft electrophile (Lewis acid), the Pd(II) shows high reactivity towards *o*-carborane and can activate the B–H bond under mild reaction conditions. As a result, we speculate whether the asymmetric Michael addition can be achieved by reacting carboranes with α,β-unsaturated carbonyl compounds under Pd(II) catalysis.

In this work, we investigate the reactions of carboranes with various α,β-unsaturated carbonyl compounds. Interestingly, the precise α-addition products are obtained by the reaction of carboranes with α,β-unsaturated carboxylic acids in the presence of $Pd(OAc)_2$ and chiral phosphoric acids (CPA) (Fig. 1e). The reaction mechanism and the origin of the enantioselectivity are studied based on experimental and computational results, revealing that the formation of a stable five-membered palladacycle intermediate is the key for the reverse selectivity. This method provides an example of the asymmetric *anti*-Michael-type addition of α,β-unsaturated carbonyl compounds. It is worth noting that this reaction shows a good B(9) selectivity for *o*/*m*-carboranes and is also suitable for *p*-carborane, resulting in a highly efficient method for the synthesis of chiral carboxylic acid units, the prevalent structural moieties in many biologically active compounds and drugs.

## Results

### Reaction establishment

To explore the proposed strategy, we chose the *m*-carborane as a model substrate because *m*-carborane shows similar reactivity to *o*-carborane

https://doi.org/10.1038/s41929-026-01480-4

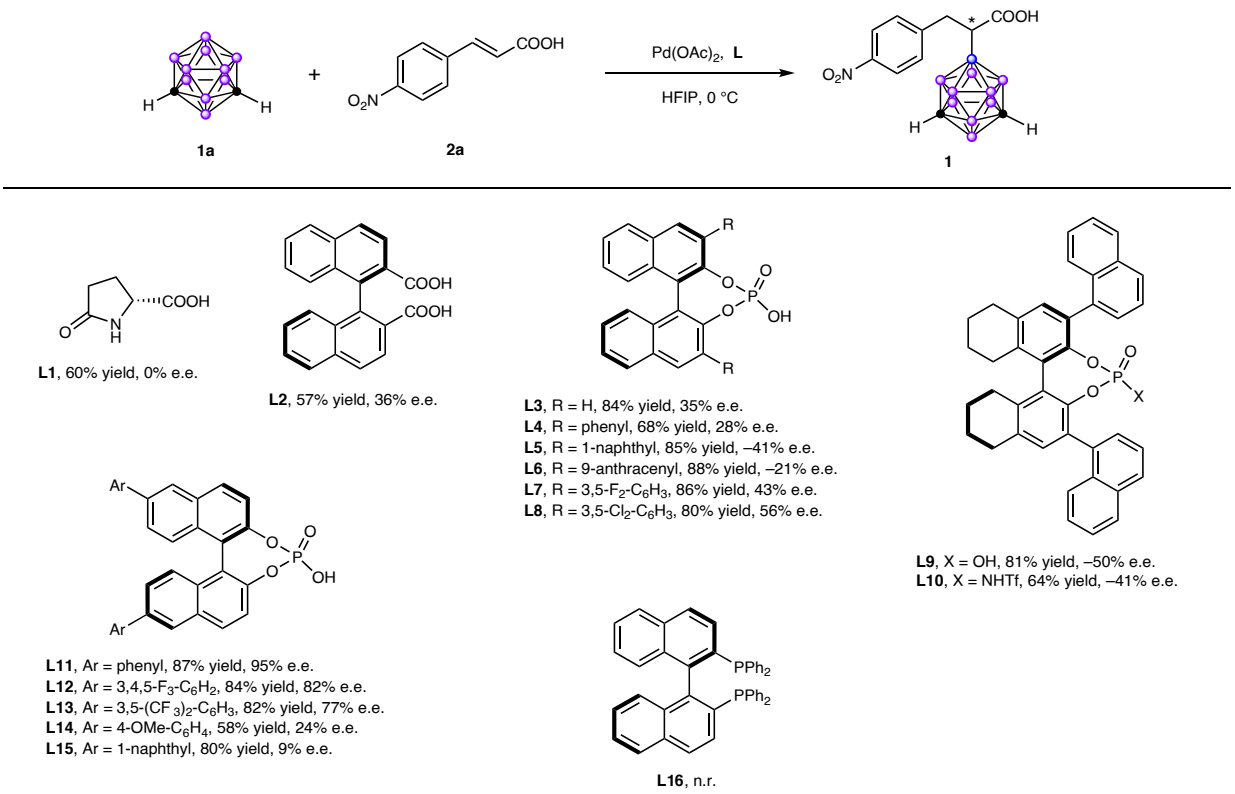


**Fig. 2 | Screening of ligands.** Reaction conditions: *m*-carborane (0,105 mmol), 4-nitrocinnamic acid (0.1 mmol), $Pd(OAc)_2$ (5 mol%) and **L** (10 mol%) in HFIP (5 ml) at 0 °C, under air atmosphere for 12 h. The isolated yields and enantioselectivities were determined by chiral HPLC analysis. n.r., no reaction.

but better selectivity in the B(9) functionalization reactions[46]. The Pd(II) catalyst shows a high reactivity towards *o*-carborane and can activate the B–H bonds under mild reaction conditions by forming a B–Pd intermediate via an electrophilic palladation process[31]. Therefore, we perceived that the catalytic asymmetric addition of α,β-unsaturated carbonyl compounds with carboranes would be able to access via Pd(II)-catalysed B–H activation. The chiral Brønsted acids, such as CPA and amino acids, widely used in asymmetric transition-metal catalysis and organic catalysis[47–51], may be suitable in this transformation; besides, solvent HFIP plays an irreplaceable role in the selective B(9)–H activation of *o*/*m*-carboranes[27–31].

Having identified the ideal system to test our hypothesized asymmetric addition method of α,β-unsaturated carboxylic acids with carboranes, diverse Brønsted acids, including chiral amino acids, carboxylic acids and phosphoric acids, were explored (Fig. 2). All the reactions proceed smoothly to give the desired product **1** in moderate to good yields. The chiral amino acids, previously reported to promote the Pd(II)-catalysed asymmetric C–H activation, only provided a racemic product in moderate yield. Pleasingly, 36% and 35% enantiomeric excess (e.e.) was detected using chiral binaphthyl dicarboxylic acid **L2** and binaphthol phosphate **L3** as ligands, and a high yield was obtained when **L3** was used. Accordingly, a series of CPA derivatives **L4**–**L15** were tested in our model reaction, suggesting that the corresponding BINOL-derived CPA bearing an aryl substituent on the 6,6′-positions is crucial for obtaining stereocontrol. Among these, the ligand 6,6′-diphenyl-binaphthol phosphate **L11** gave the best result (87% yield and 95% e.e.). Ligands with a strong coordination ability, such as BINAP, failed to provide any desired product, demonstrating that an electron-deficient Pd(II) catalyst is required to initiate this transformation.

## Scope of α,β-unsaturated carboxylic acids

The generality of this Pd(II)-catalysed asymmetric *anti*-Michael-type addition reaction was examined by varying the structure of α,β-unsaturated carboxylic acids (Fig. 3). First, the commercially available cinnamic acid derivatives were scrutinized, and the results indicated that various functional groups at the *para*-, *meta*- and *ortho*-positions were compatible, affording the desired products **1**–**25** in moderate to excellent yields and 71–95% e.e. Cinnamic acids containing an electron-deficient group on the phenyl gave a better result in both yields and enantioselectivities. By contrast, no product was detected for the electron-donating one (**15**). It is particularly noteworthy that boronate and the formyl groups remain intact in this reaction. *N*-heteroaryl substituted α,β-unsaturated carboxylic acids were then investigated, and no corresponding products were detected under the standard reaction conditions, presumably due to the strong coordination effect of the nitrogen atom, thus decreasing the electrophilicity of the Pd(II) catalyst. As a result, Brønsted acid trifluoromethanesulfonic acid (HOTf) was added to the reaction system to protect the nitrogen atom, and as expected, the products **26** and **27** were obtained in 70% and 60% yields, respectively, with moderate enantioselectivities. Next, we tested the β-alkyl-substituted acrylic acids, revealing that a long alkyl chain is beneficial for the enantioselectivities (**28**–**30**). Royal jelly acid and its derivative were suitable substrates, forming products **31** and **32** in 55% and 82% yields, along with 76% and 77% enantioselectivities. Asymmetric addition of large steric isopropyl substituted acrylic acid gave the desired product **33** in low yield and e.e. value. Next, α,β-unsaturated carboxylic acids with an electron-deficient group on the β position were examined, and the carboranyl group was still introduced to the α-stereocentre of carboxylic acid when 3-ethoxylacrylic acid and 3-chloroacrylic acid were used (**34**, **35**). A mixture of α- and β-carboranyl carboxylic acids was detected when 3-trifluoromethylacrylic acid was subjected to the reaction system, and the major product α-carboranyl carboxylic acid **36** was isolated in 32% yield with 75% e.e. value. The absolute structure of **36** was further determined by X-ray single crystal diffraction.

https://doi.org/10.1038/s41929-026-01480-4

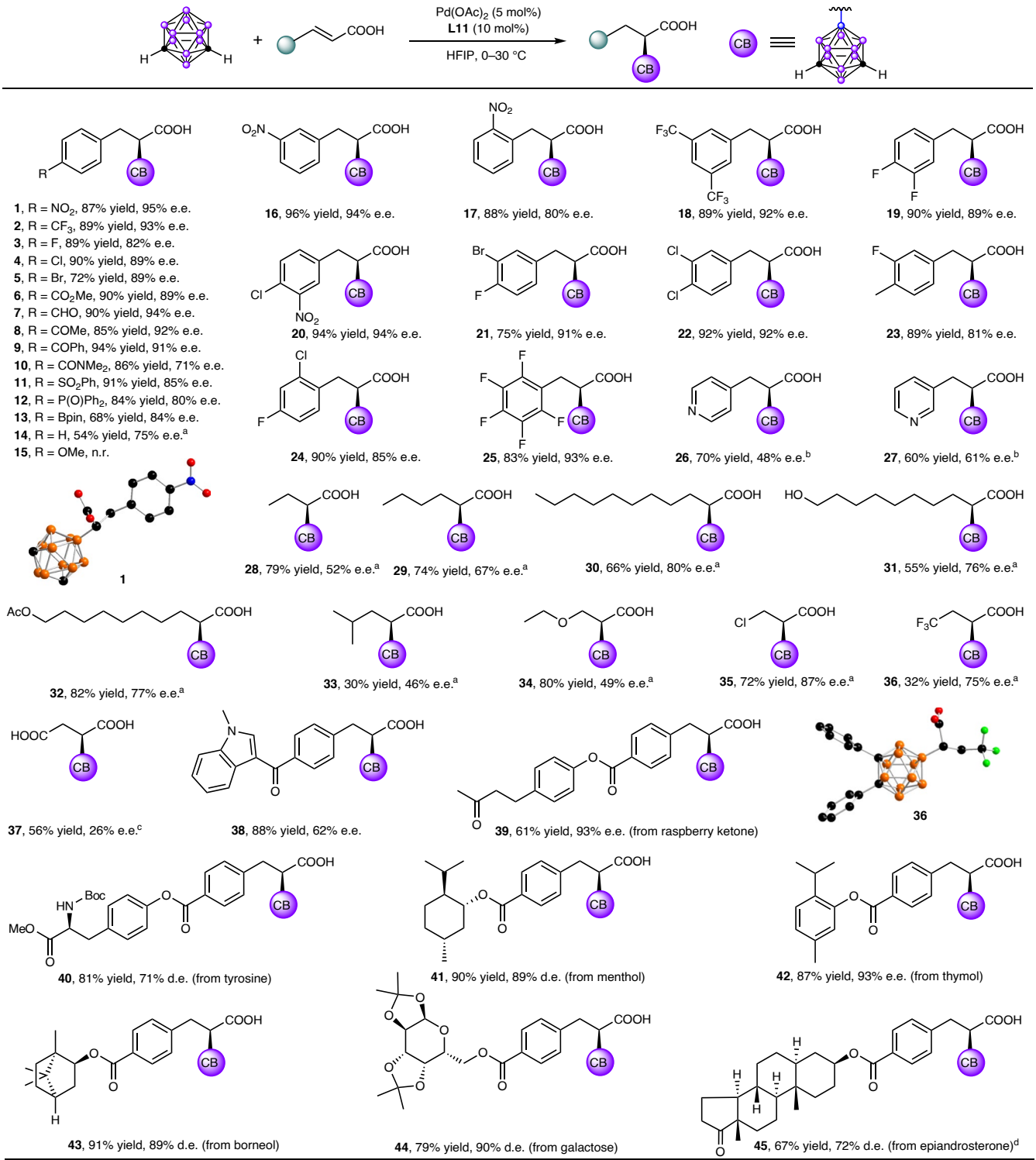


**Fig. 3 | Scope of α,β-unsaturated carboxylic acids.** Reaction conditions: *m*-carborane (0.105 mmol), α,β-unsaturated carboxylic acid (0.1 mmol), $Pd(OAc)_2$ (0.005 mmol, 5 mol%), **L11** (0.01 mmol, 10 mol%) in HFIP (5 ml), air atmosphere, isolated yields, the e.e. and d.e. values were determined by chiral HPLC. [a]1,2-$Ph_2$-*o*-carborane was used as the substrate, and 1 ml DCM was added. [b]HOTf (1.05 equiv.) was used. [c]1,2-Bis(2-fluorophenyl)-*o*-carborane was used at 30 °C for 24 h, then at 60 °C for 12 h. [d]10 mol% $Pd(OAc)_2$ and 12 mol% **L11** were used in HFIP (1 ml). n.r., no reaction; d.e., diastereomeric excess.

Unfortunately, the β-carboranyl carboxylic acid was not obtained in pure form. Symmetric fumaric acid gave the desired product **37** in moderate yield with a low e.e. value. The highly functional group tolerance prompted us to explore the potential of late-stage modification of biorelevant molecules. A series of bioactive molecules and natural products, including indole, raspberry ketone, epiandrosterone, tyrosine, menthol, thymol, borneol and galactose, were derivatized into the cinnamic acid and then were put into the system. All the reactions worked well to deliver the target products **38**–**45** in good to excellent yields, and the substituents on the carbonyl group significantly influenced the enantioselectivity, resulting in the e.e. values ranging from 62% to 93%.

https://doi.org/10.1038/s41929-026-01480-4

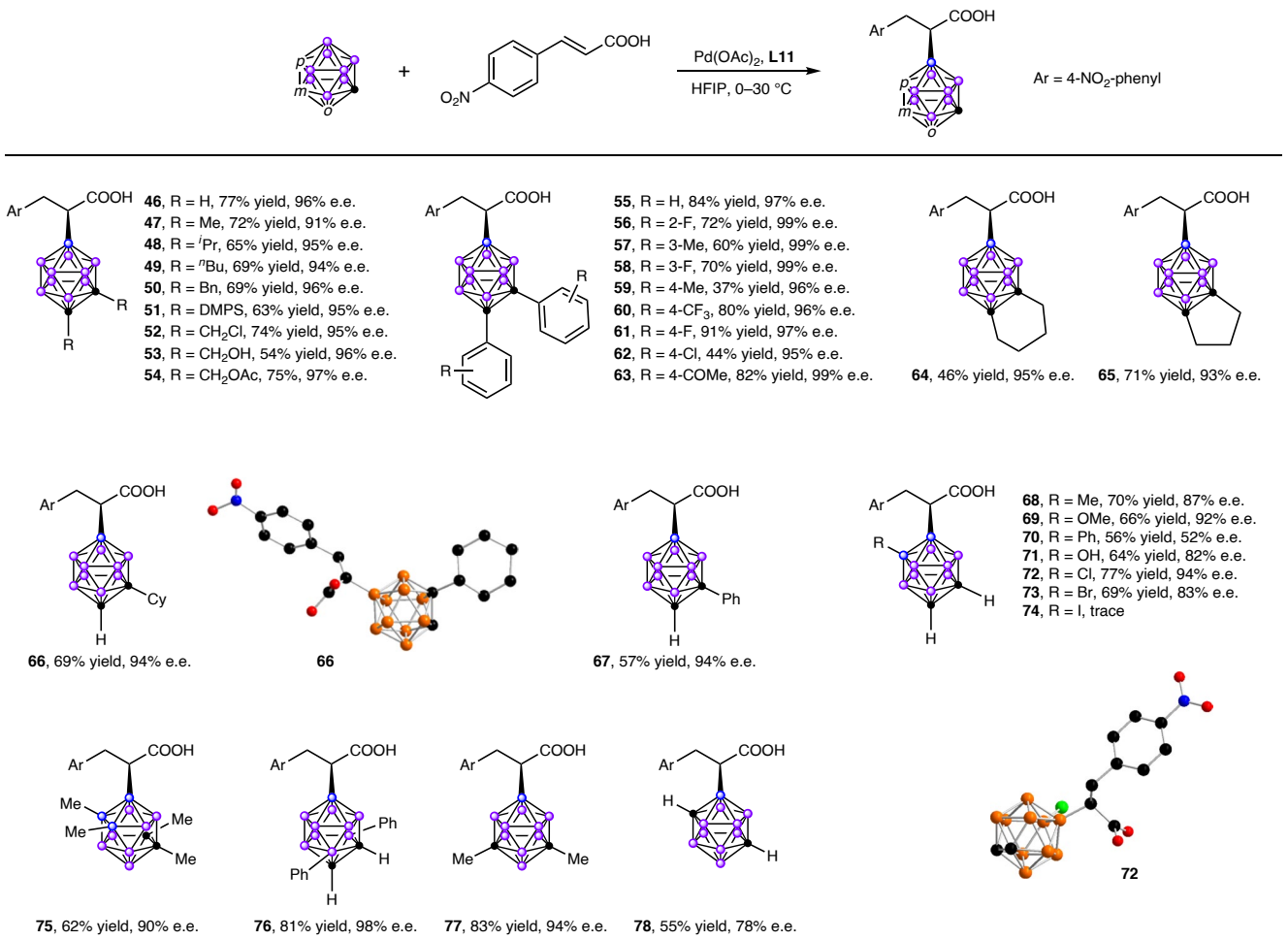


**Fig. 4 | Scope of carboranes.** Reaction conditions: carborane (0.105 mmol), 4-nitrocinnamic acid (0.1 mmol), $Pd(OAc)_2$ (0.005 mmol, 5 mol%), **L11** (0.01 mmol, 10 mol%) in HFIP (5 ml), air atmosphere. The isolated yields and the e.e. values were determined by chiral HPLC.

## Scope of carboranes

Next, we investigated the scope of carboranes (Fig. 4). Similar to *m*-carborane, the reaction of *o*-carborane formed the desired product **46** with 77% yield and 96% e.e. and a good B(9) selectivity (a B9/B8 ratio of 9:1 based on $^{11}B\{^1H\}$ nuclear magnetic resonance (NMR) and high-performance liquid chromatography (HPLC)) (see Supplementary Fig. 3 and Supplementary Table 5 for details). Encouraged by this result, we examined the scope of *o*-carboranes. A broad range of di-*C*-substituted *o*-carboranes afforded target products **47**–**65** in moderate to good yields (37–91%) and excellent e.e. (91–99%). Product **51** was obtained in 63% yield and 95% e.e. with the silyl group remained intact, a stark contrast to the typical elimination of silyl moieties observed in a Pd(II)-catalysed B–H activation[31]. Notably, *C*-aryl substituted *o*-carboranes delivered the desired products **55**-**63** in high enantioselectivities, and up to 99% e.e. was gained. The asymmetric alkylation of mono-*C*-substituted *o*-carboranes provided a mixture of B(8), B(9), B(10) and B(12) products, and the major B(9) products **66** and **67** were isolated in 69% and 57% yields, respectively, still with excellent enantioselectivity. The absolute configuration of compound **66** was unambiguously established via X-ray crystallographic characterization. In contrast to *C*-substituted *o*-carboranes, substituents on the boron vertexes have a significant influence on both the yields and enantioselectivities (**68**–**74**), such as only 52% e.e. of **70** was provided when 9-Ph-*o*-carborane was used, and the substrate with an iodine atom at B(9) position was ineffective in this reaction. The *o*-carborane containing substituents on both of the B(9) and B(12) vertices was also compatible, affording the corresponding B(8)-product **75** in 62% yield and 90% e.e. The substrate bearing substituents at B(3,6) vertices performed well, forming the desired product **76** in 81% yield and 98% e.e. 1,7-$Me_2$-*m*-carborane was then subjected to the reaction system, providing product **77** in 83% yield and 94% e.e. Given the fact that the present protocol provides an efficient reaction platform to introduce carboranes to the α-*C*-chiral centre of carboxylic acids, *p*-carborane, which is much more inert than *o*-carborane and *m*-carborane, was explored, yielding the desired product **78** in 55% yield and 78% e.e.

## Synthetic applications

The robustness and scalability of this reaction were verified by a large-scale reaction of *o*-carborane with 4-nitrocinnamic acid, which afforded the corresponding product **46** in 86% yield and 93% e.e. (Fig. 5a). The carborane derivatives are excellent candidates for use in boron neutron capture therapy, but only the $^{10}B$ atom was effective. Therefore, $^{10}B$-enriched *o*-carborane was subjected to the reaction, and the corresponding $^{10}B$-enriched **$^{10}$B-46** was obtained in 90% yield and 95% e.e. (Fig. 5b). To demonstrate the practicality of our methodology, we examined the derivatization of the carboxyl and nitro groups (Fig. 5c). Reduction of **46** with THF·$BH_3$ delivered alcohol **79** in 85% yield with no erosion of enantiomeric excess. Ester **80** was obtained in 87% yield still with no decrease of e.e. by the reaction of **46** and EtOH in the presence of HOTf. Amido linkage was constructed by treating **46** with glycine methyl ester hydrochloride, affording **81** in 53% yield and 93% e.e. The nitro group was selectively reduced to an amido group with

https://doi.org/10.1038/s41929-026-01480-4

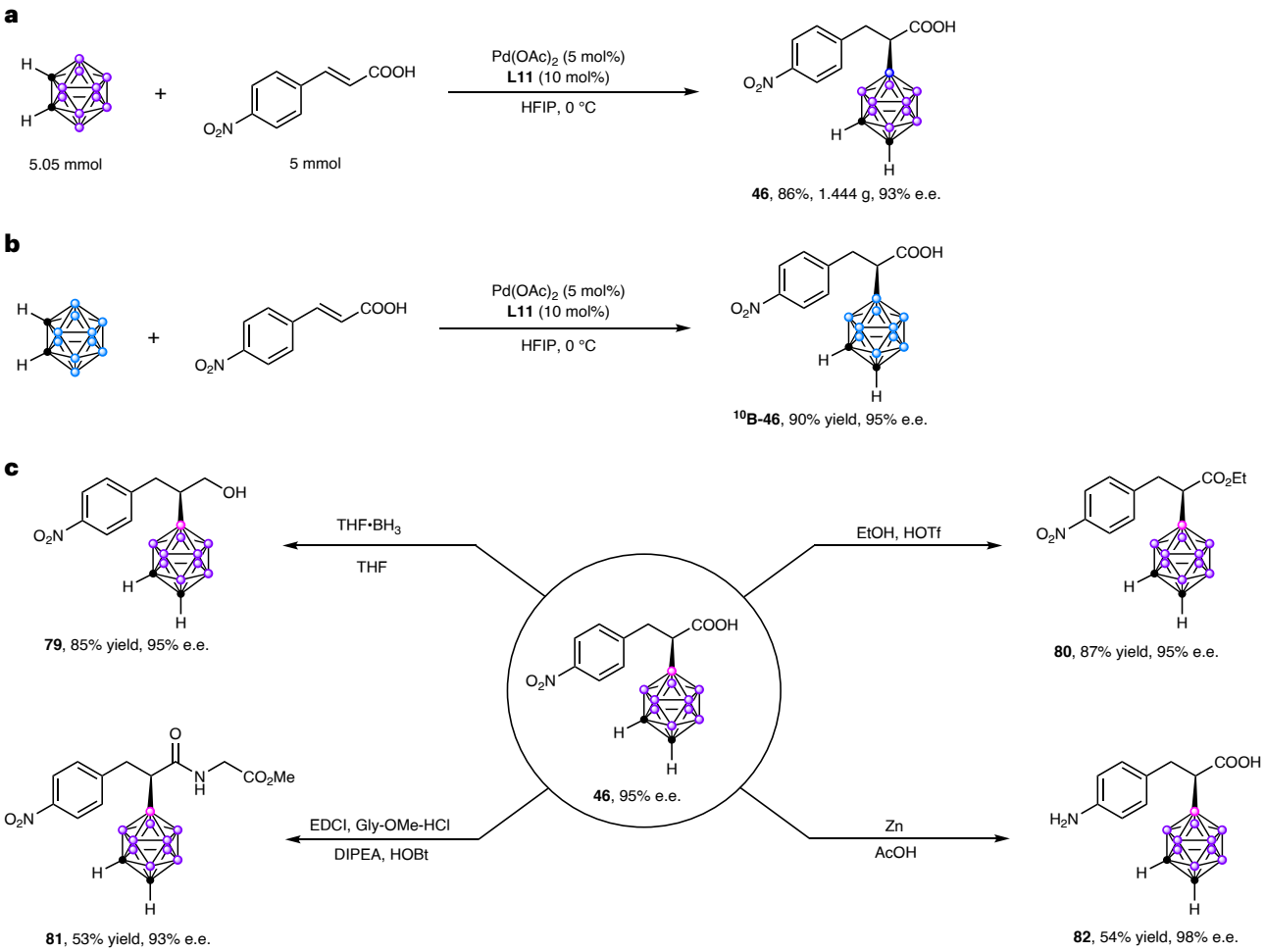


**Fig. 5 | Synthetic applications. a**, Gram-scale reaction. **b**, Synthesis of $^{10}$B-labelled product. **c**, Transformations of chiral α-carboranyl carboxylic acids.

zinc powder in acetic acid, giving the product **82** in 54% yield and 98% e.e. The maintenance of the enantioselectivity in all these transformations indicates that the C-stereocentre was stable towards both acids and bases.

## Mechanistic studies

Control experiments have been conducted to gain insight into the reaction mechanism. Switching (*E*)-4-$NO_2$-cinnamic acid to its (*Z*)-isomer, the enantioselectivity was dramatically reduced (Fig. 6a(i)), suggesting the (*E*)-configuration was necessary to obtain high enantioselectivity. Next, the cinnamic acid derivatives cinnamate and cinnamamide were investigated. The reactions proceeded smoothly to form the corresponding products **80** and **83** in 89% and 75% yields, respectively, but with only 33% and 17% e.e. (Fig. 6a(ii)). Racemic **46** was isolated in 69% yield in the absence of any of the ligands, but only trace amount of products **80** and **83** were detected under the same reaction conditions (Fig. 6a(iii)). These results illustrated that an acidic proton is necessary to achieve this transformation. To support this conclusion, 1 equivalent HOAc was added to the reaction systems of cinnamate or cinnamamide, and the desired products **80** or **83** were obtained in 20% and 18% yields, respectively (Fig. 6a(iv)). Next, the deuterium-labelling experiments were conducted to determine the source of the hydrogen atom on the β position (Fig. 6b). First, DOAc was added to the reaction system, and the results suggested that the deuterium atom of DOAc was not transferred to the product even when 10 equiv. DOAc was used (Fig. 6b(i)). A similar result was detected using $D_2O$ to instead DOAc (Fig. 6b(ii)). Notably, the introduction of DOAc and $D_2O$ does not influence the yield and e.e. value, suggesting that this reaction is robust. Subjecting B(8,9,10,12)-$D_4$-*o*-carborane to the optimized reaction conditions revealed that deuterium incorporates solely at the β position via a *syn*-addition process, and a 41% deuterium incorporation degree was detected (Fig. 6b(iii)). Interestingly, H/D exchange on the boron vertexes was observed, and the deuterium incorporation levels on all the boron vertexes were similar, which suggested that a Pd-migration process should be included under standard reaction conditions[52]. Encouraged by these results, *o*-carborane with perdeuteration on the boron vertexes (90% D on all boron vertexes) was subjected to the reaction and the deuterium atom was transformed to the β position of α,β-unsaturated carboxylic acid via a *cis* addition (Fig. 6b(iv)). All these results indicate that the deuterium atom on the β position comes from the carborane. A kinetic isotope effect of 3.5 was observed in the parallel kinetic experiment, suggesting that breaking the B–H bond was the rate-determining step (Fig. 6b(v)). It is worth noting that a co-solvent of HFIP/DCM (v/v = 9:1) was used to guarantee the substrates *o*-carborane and deuterated *o*-carborane were fully soluble because of the low solubility of *o*-carborane in HFIP. The one-pot competing experiment was also conducted and a kinetic isotope effect of 3.0 was observed (Supplementary Figs. 15 and 16). Unexpectedly, 25% and 50% deuterium incorporation degrees on the β position and the boron vertexes of the desired product were observed, respectively. We speculated that an intermolecular H/D exchange on the boron vertexes of *o*-carborane should be included in this transformation. To validate our speculation, we conducted intramolecular and intermolecular H/D exchange experiments (Fig. 6b(vi),(vii)). As expected, the deuterium atoms were

https://doi.org/10.1038/s41929-026-01480-4

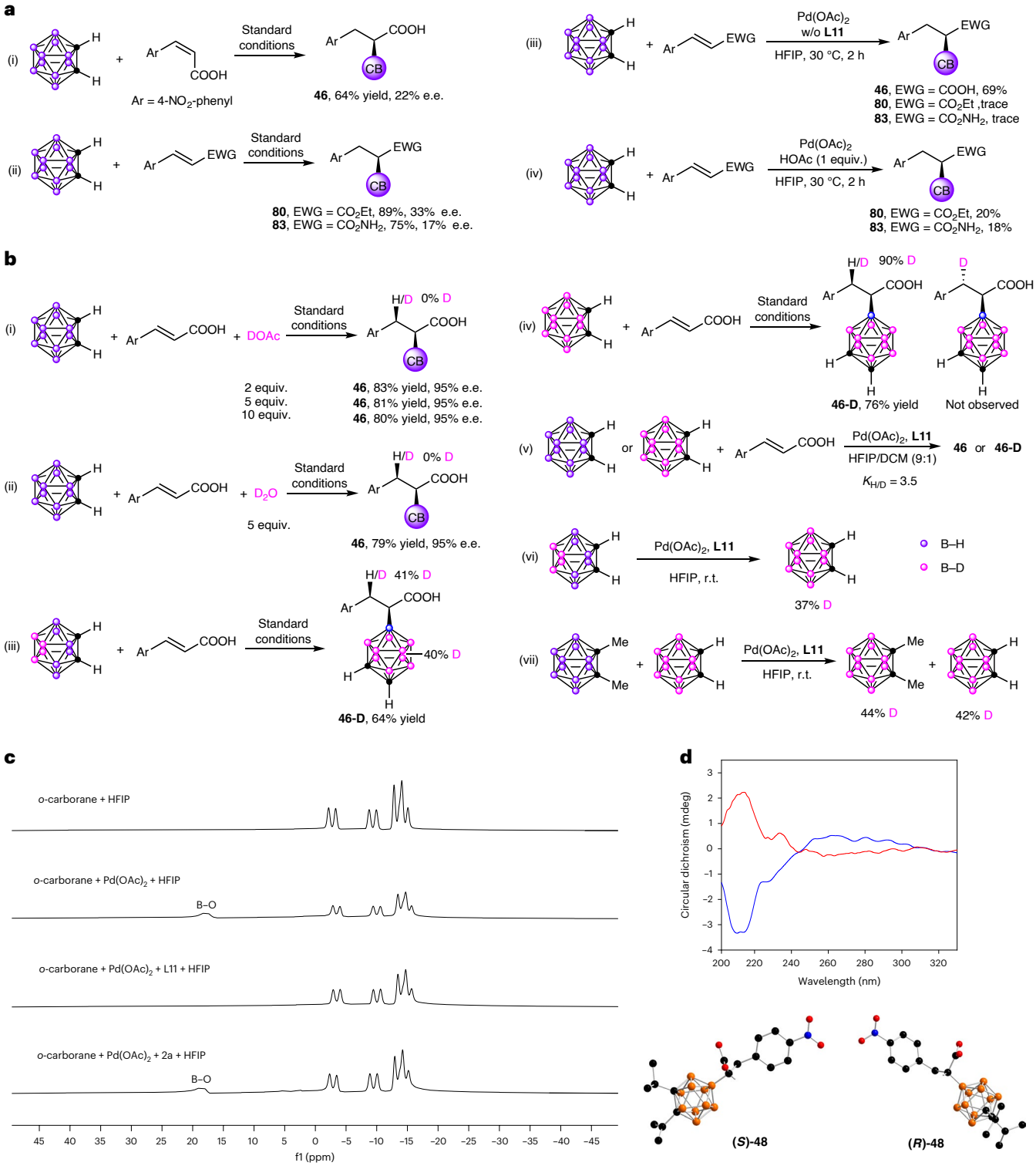


**Fig. 6 | Mechanistic studies. a**, Control experiments. **b**, Deuterium-labelling experiments. **c**, $^{11}$B NMR of different composites. **d**, Circular dichroism spectra of (***S***)-**46** (blue) and (***R***)-**46** (red) in $CH_3CN$ ($c$ = 0.1 mg ml$^{-1}$) and molecular structures of (***S***)-**48** and (***R***)-**48**. r.t., room temperature. Standard conditions, $Pd(OAc)_2$ (0.005 mmol, 5 mol%), L11 (0.01 mmol, 10 mol%) in HFIP (5 ml), Supplementary Information for details. EWG, electron-withdrawing group; f1, chemical shift axis label of the indirect dimension.

distributed equally to all the boron vertexes. To further explore the reaction mechanism, some $^{11}$B NMR (Fig. 6c) were detected, which suggested that *o*-carborane quickly decomposed under $Pd(OAc)_2$ catalyst in HFIP by forming a B–Pd intermediate, then reductive elimination to give the B–O coupling products. By contrast, the decomposition was inhibited in the presence of CPA by forming a counteranion B–Pd–**L11**.

Circular dichroism spectra of (*S*)-**46** and (*R*)-**46** obtained with (*R*)-**L11** and (*S*)-**L11** exhibited unambiguously mirror images to each other, indicating a pair of enantiomers (Fig. 6d). Furthermore, the absolute configuration of (*S*)-**48** and (*R*)-**48** was confirmed by X-ray crystallography.

The density functional theory (DFT) calculations by using the Gaussian 16[53] program have been carried out for exploring the

https://doi.org/10.1038/s41929-026-01480-4

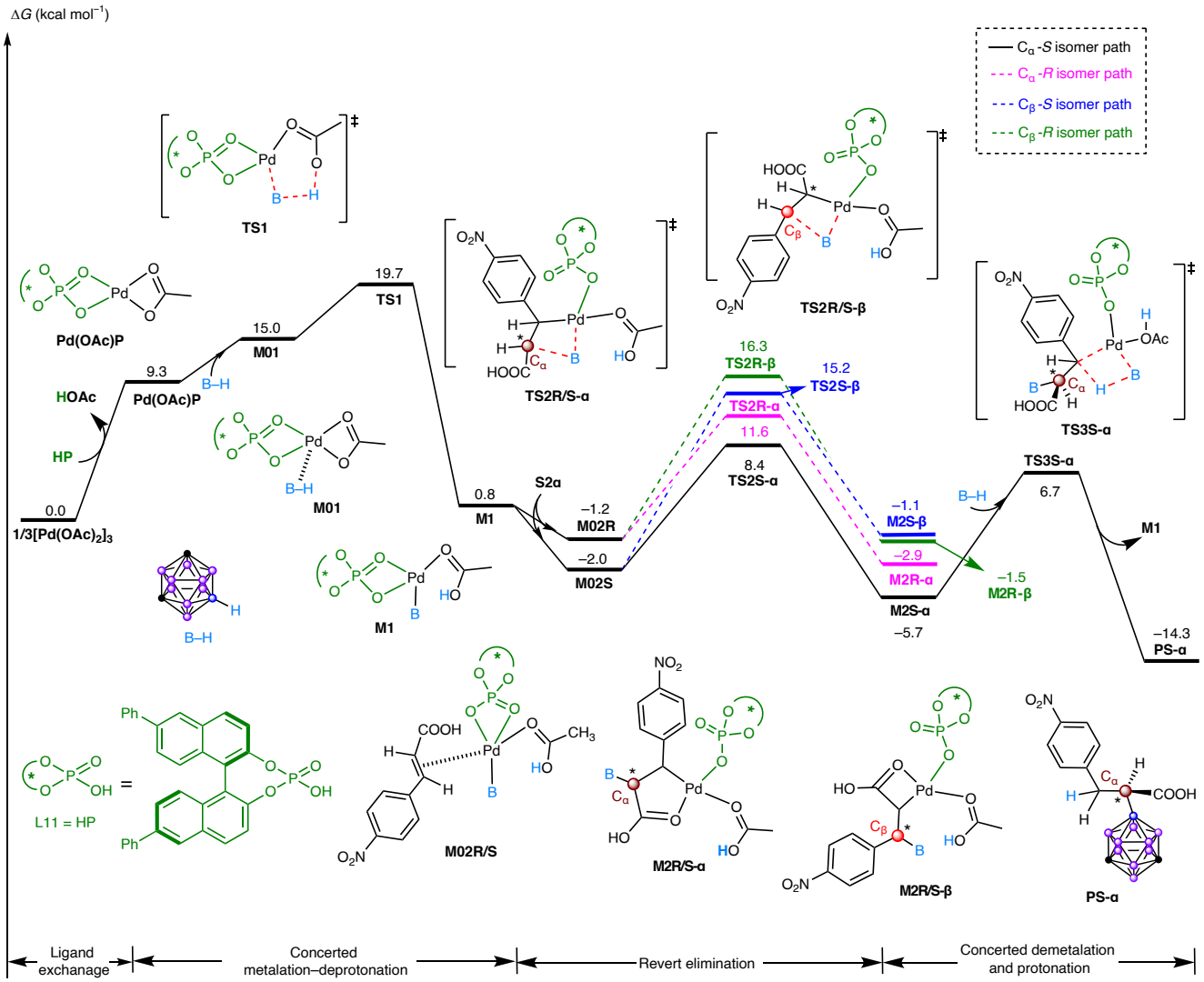


**Fig. 7 | DFT calculations.** Relative Gibbs free energy profiles for the possible regio- and stereoselective pathways computed at the M06-L/SDD$_{(Pd)}$/6-311++G(d, p)/IEF-PCM$_{(HFIP)}$//M06-L/Lanl2DZ$_{(Pd)}$/6-31G(d, p)/IEF-PCM$_{(HFIP)}$ level.

mechanisms and origin of stereoselectivity of the Pd-catalysed reaction. Three possible pathways for the formation of regioselective products **P-α** and **P-β**, including concerted metalation–deprotonation (CMD), concerted hydride-transfer and the Pd–B bond formation and the B–H insertion for the formation of the Pd–H species, have been considered and investigated in theory. In Fig. 7, we provided the possible CMD pathway. First, the metallic palladium in intermediate **M01** activates the B–H bond of carborane to form intermediate **M1** through a CMD transition state **TS1** ($\Delta G^{\ddagger}$ = 19.7 kcal mol$^{-1}$). Then, α-selective intermediates **M2S-α** and **M2R-α** can be formed through C–B bond formation transition states **TS2S-α** ($\Delta G^{\ddagger}$ = 10.4 kcal mol$^{-1}$) and **TS2R-α** ($\Delta G^{\ddagger}$ = 12.8 kcal mol$^{-1}$), respectively. Alternatively, β-selective intermediates, **M2S-β** and **M2R-β**, can be formed through C–B bond formation transition states **TS2S-β** ($\Delta G^{\ddagger}$ = 17.2 kcal mol$^{-1}$) and **TS2R-β** ($\Delta G^{\ddagger}$ = 17.5 kcal mol$^{-1}$), respectively. Finally, the product **PS-α** is obtained through a concerted demetalation and protonation transition state **TS3S-α** ($\Delta G^{\ddagger}$ = 12.4 kcal mol$^{-1}$). Moreover, other possible CMD pathways were also considered and excluded in Supplementary Fig. 36. The computed results indicate that the α-selective pathway associated with *S*-isomer should be the most energetically favourable pathway, which is consistent with the experimental results.

In addition, we have considered other two possible kinds of pathways for the catalytic reaction, including concerted hydride-transfer and Pd–B bond formation pathway as well as B–H insertion pathway associated with formation of Pd–H species (Supplementary Fig. 34). In the concerted hydride-transfer and Pd–B bond formation pathway, first, the metal palladium in intermediate **M1′α-S** activates the B–H bond of carborane, forming intermediate **M2′α-S** through a proton transfer transition state **TS1′α-S** ($\Delta G^{\ddagger}$ = 43.5 kcal mol$^{-1}$). Then, **M3′α-S** can be generated through a C–B bond formation transition state **TS2′α-S** ($\Delta G^{\ddagger}$ = 43.9 kcal mol$^{-1}$). Alternatively, the proton transfer process occurs from **M1′α-R** to form **M2′α-R** through transition state **TS1′α-R** ($\Delta G^{\ddagger}$ = 44.7 kcal mol$^{-1}$). Subsequently, **M3′α-R** is generated through the other C–B bond formation transition state **TS2′α-R** ($\Delta G^{\ddagger}$ = 45.4 kcal mol$^{-1}$). Based on the formation mechanism of metal hydrides[54], we have also considered and located a B–H insertion transition state **TS1-1** ($\Delta G^{\ddagger}$ = 25.4 kcal mol$^{-1}$) in Supplementary Fig. 34. Since the energy barrier of transition state **TS1-1** is higher than that of CMD transition state **TS1** ($\Delta G^{\ddagger}$ = 19.7 kcal mol$^{-1}$), the B–H insertion pathway associated with formation of Pd–H species can be excluded. Comparative analysis of energy barriers across various pathways revealed that the β-selective paths are energetically unfavourable and should be excluded in theory. By contrast, the *S*-configurational pathway associated with α-selective path in the CMD mechanism exhibits the lowest energy barrier, which agrees with the experimental observations of stereoselectivity and regioselectivity.

https://doi.org/10.1038/s41929-026-01480-4

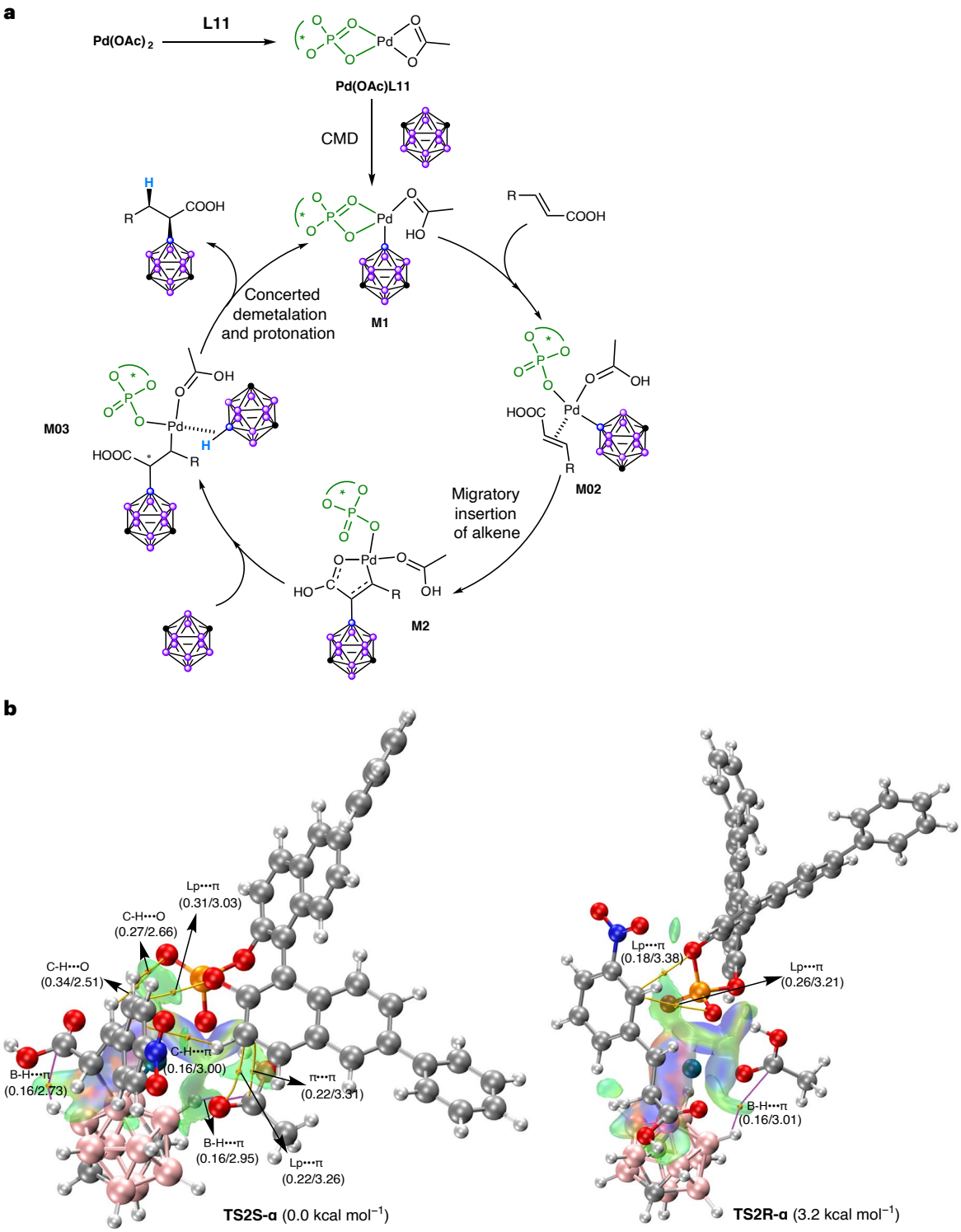


**Fig. 8 | Proposed mechanism. a**, Proposed catalytic cycle. **b**, Qualitative and quantitative non-covalent interaction analyses for the stereocontrol of transition states **TS2S-α** and **TS2R-α** (blue, green and red represent strong and weak interactions and steric hindrance, respectively; the distances are measured in Ångström, and the values of Laplacian of electron densities ($\nabla^2\rho$ in $10^{-1}$ a.u.) in atomic units) and distances (unit in Ångström) in the parentheses. The red, blue, grey, white, pink, orange and green spheres represent oxygen, nitrogen, carbon, hydrogen, boron, phosphorus and palladium atoms in the three-dimensional structure, respectively.

Notably, only a trace amount of product **1** was obtained when $Pd(TFA)_2$ instead of $Pd(OAc)_2$ was used as the catalyst (Supplementary Table 3, entry 2). However, upon adding bases such as NaOAc, PhCOONa or $NaHCO_3$, or the sodium salt of **2a**, to the reaction system, the target product **1** can be obtained with moderate yields and e.e. values (Supplementary Table 3, entries 3–6). This result indicates that the activation of the B–H bond indeed proceeds via the CMD mechanism. Meanwhile, it also confirms that Pd(**S2**)**L11** can also act as an active catalyst to activate the B–H bond but gave a lower reactivity and enantioselectivity compared with Pd(OAc)**L11**.

To further support the DFT calculation results, we measured the kinetic order for each reaction component (see Supplementary Information for details). As expected, the reaction exhibits first order to carborane, CPA and catalyst, and an inverse order to α,β-unsaturated carboxylic acid (Supplementary Figs. 31–33). These kinetic data suggest that carborane, palladium catalyst, and CPA were involved in the turnover-limiting step. The inverse order dependence on the α,β-unsaturated carboxylic acid can be attributed to the lower reactivity of the formed α,β-unsaturated carboxylic acid anion-coordinated palladium catalyst Pd(**S2**)**L11** compared with the acetate anion-coordinated palladium catalyst Pd(OAc)**L11** (Supplementary Fig. 35). This leads to a slower reaction rate and a decreased e.e. value. For example, the e.e. value was reduced to 83% from 94% for product **7** when 2 equiv. 4-formylcinnamic acid was used (see Supplementary Table 11 for details).

Based on the experimental and computational results, a plausible reaction mechanism is depicted in Fig. 8a. Reaction of $Pd(OAc)_2$ with CPA **L11** generates the chiral catalyst **Pd(OAc)L11**. Then B–H activation via a CMD process formed intermediate **M1**. Subsequently, alkene coordination and migratory insertion of the alkene moiety into the Pd–B bond give a five-membered palladacycle **M2**. Finally, the desired product was formed via carborane coordination and concerted demetalation and protonation, whereby the hydrogen atom on the carborane is transferred to the β position. The formation of a stable five-membered palladacycle **M2** is key to the α-selectivity of the reaction.

To elucidate the source and determining factor of stereoselectivity, we conducted further qualitative non-covalent interactions analysis and quantitative atom-in-molecules analyses[55] for the key transition states **TS2S-α** and **TS2R-α**, in which the two chiral carbons are formed independently. The results showed that the weak B–H···π (ref. 56) and lone-pair (LP)···π interactions existing in **TS2S-α** are considerably stronger than the corresponding interactions in **TS2R-α**. Notably, the olefin substrates within **TS2S-α** participates in a variety of weak interactions, whereas no C–H···π, π···π and C–H···O interactions are established between the olefin substrate and the reaction system in **TS2R-α**. Collectively, the weak interactions in **TS2S-α** are more and stronger than those observed in **TS2R-α**, which leads to that the *S*-configurational pathway associated with **TS2S-α** is more energetically favourable.

## Conclusion

In summary, a Pd(II)-catalysed asymmetric *anti*-Michael-type addition reaction of α,β-unsaturated carboxylic acids with carboranes using CPA as a ligand has been established. A series of α,β-unsaturated carboxylic acids ranging from cinnamic acid and corresponding derivatives to alkyl-substituted acrylic acids are effective substrates in this protocol, leading to the formation of α-carboranyl carboxylic acids in high yields and enantioselectivities. The experimental and computational studies have elucidated the reaction mechanism and origin of the enantioselectivity. This highly selective *anti*-Michael-type addition reaction provides a general and straightforward method to introduce *o*-, *m*- and *p*-carboranes to the α-carbon-stereocentre of carboxylic acids under mild reaction conditions. Our ongoing efforts in the laboratory involve more detailed mechanistic investigations and the expansion of the nucleophile and alkene scope.

## Methods

### General protocol for the asymmetric palladium-catalysed asymmetric α-addition of α,β-unsaturated carboxylic acids with carboranes

In a 10 ml Schlenk tube was added carborane (0.105 mmol, 1.05 equiv.), α,β-unsaturated carboxylic acid (0.1 mmol, 1.0 equiv.), **L11** (0.01 mmol, 10 mol%), $Pd(OAc)_2$ (0.005 mmol, 5 mol%) and HFIP (5 ml). The resulting mixture was stirred at 0 °C for 10 h under air atmosphere. Then the reaction was warmed up to room temperature and stirred continuously until the reaction was complete. The solvent HFIP was removed under reduced pressure, and the residue was subjected to flash column chromatography on silica gel (200–300 mesh) to give the pure product.

### Computational details

All computations were performed with the Gaussian 16 program by using DFT, and the geometries were fully optimized at the solution phase (HFIP as solvent) with the integral equation formalism polarizable continuum model (IEF-PCM) solvation model. The internal parameters static dielectric constant ($\varepsilon = 16.7$) was used to define the HFIP solvent. The M06-L functional with Lanl2DZ and 6-31G(d, p) was used for geometry optimization involved in the model reaction. Moreover, single-point energy calculations were performed at the M06-L/$SDD_{(Pd)}$/6-311++G(d, p)/IEF-$PCM_{(HFIP)}$ level. The discussed energies were obtained at the M06-L/$SDD_{(Pd)}$/6-311++G(d, p)/IEF-$PCM_{(HFIP)}$//M06-L/$Lanl2DZ_{(Pd)}$/6-31G(d, p)/IEF-$PCM_{(HFIP)}$ level. In addition, we used Multiwfn and VMD to draw the pictures of the three-dimensional structures of transition states, as well as the non-covalent interactions and atom-in-molecules analyses.

## Data availability

Crystallographic data for compounds **1**, **36**, (***S***)-**48**, (***R***)-**48**, **66** and **72** have been deposited at the Cambridge Crystallographic Data Centre under deposition numbers CCDC 2380830-2380835. Additional optimization, experimental procedures, characterization of compounds and all other data supporting the findings are available in the Supplementary Information and from the corresponding author upon request.

## References

1. Grimes, R. N. *Carboranes* 3rd edn (Elsevier, 2016).
2. Marfavi, A., Kavianpour, P. & Rendina, L. M. Carboranes in drug discovery, chemical biology and molecular imaging. *Nat. Rev. Chem.* **6**, 486–504 (2022).
3. Stockmann, P., Gozzi, M., Kuhnert, R., Sárosi, M. B. & Hey-Hawkins, E. New keys for old locks: carborane-containing drugs as platforms for mechanism-based therapies. *Chem. Soc. Rev.* **48**, 3497–3512 (2019).
4. Ochi, J., Tanaka, K. & Chujo, Y. Recent progress in the development of solid-state luminescent o-carboranes with stimuli responsivity. *Angew. Chem. Int. Ed.* **59**, 9841–9855 (2020).
5. Ready, A. D., Nelson, Y. A., Pomares, D. F. T. & Spokoyny, A. M. Redox-active boron clusters. *Acc. Chem. Res.* **57**, 1310–1324 (2024).
6. He, T., Klare, H. F. T. & Oestreich, M. Arenium-ion-catalysed halodealkylation of fully alkylated silanes. *Nature* **623**, 538–543 (2023).
7. Kona, C. N. et al. Aromatic halogenation using carborane catalyst. *Chem.* **10**, 402–413 (2024).
8. Hawthorne, M. F. & Maderna, A. Applications of radiolabeled boron clusters to the diagnosis and treatment of cancer. *Chem. Rev.* **99**, 3421–3434 (1999).
9. Issa, F., Kassiou, M. & Rendina, L. M. Boron in drug discovery: carboranes as unique pharmacophores in biologically active compounds. *Chem. Rev.* **111**, 5701–5722 (2011).
10. Xu, Y., Yang, Y., Liu, Y., Li, Z. & Wang, H. Boron-catalysed hydrogenolysis of unactivated C(aryl)–C(alkyl) bonds. *Nat. Catal.* **6**, 16–22 (2023).
11. Keener, M. et al. Redox-switchable carboranes for uranium capture and release. *Nature* **577**, 652–655 (2020).
12. Bawari, D., Toami, D., Jaiswal, K. & Dobrovetsky, R. Hydrogen splitting at a single phosphorus centre and its use for hydrogenation. *Nat. Chem.* **16**, 1261–1266 (2024).
13. Ma, W. et al. Luminescence modulation in boron-cluster-based luminogens via boron isotope effects. *Angew. Chem. Int. Ed.* https://doi.org/10.1002/anie.202410430 (2024).

14. Qiu, Z. & Xie, Z. Functionalization of *o*-carboranes via carboryne intermediates. *Chem. Soc. Rev.* **51**, 3164–3180 (2022).
15. Liu, Q. et al. Visible-light-induced photoreduction of carborane phosphonium salts: efficient synthesis of carborane-oxindole-pharmaceutical hybrids. *Angew. Chem. Int. Ed.* **62**, e202305088 (2023).
16. Spokoyny, A. M. et al. A coordination chemistry dichotomy for icosahedral carborane-based ligands. *Nat. Chem.* **3**, 590–596 (2011).
17. Yu, W.-B., Cui, P.-F., Gao, W.-X. & Jin, G.-X. B–H activation of carboranes induced by late transition metals. *Coord. Chem. Rev.* **350**, 300–319 (2017).
18. Quan, Y. & Xie, Z. Controlled functionalization of *o*-carborane via transition metal catalyzed B–H activation. *Chem. Soc. Rev.* **48**, 3660–3673 (2019).
19. Zhang, X. & Yan, H. Transition metal-induced B–H functionalization of *o*-carborane. *Coord. Chem. Rev.* **378**, 466–482 (2019).
20. Qiu, Z. & Xie, Z. A strategy for selective catalytic B–H functionalization of *o*-carboranes. *Acc. Chem. Res.* **54**, 4065–4079 (2021).
21. Yang, L., Zhang, Z.-J., Jei, B. B. & Ackermann, L. Electrochemical cage activation of carboranes. *Angew. Chem. Int. Ed.* **61**, e202200323 (2022).
22. Ren, H. et al. Dative bonding activation enables precise functionalization of the remote B–H bond of *nido*-carborane clusters. *J. Am. Chem. Soc.* **146**, 26543–26555 (2024).
23. Xu, S. et al. Photoinduced selective B–H activation of *nido*-carboranes. *J. Am. Chem. Soc.* **146**, 7791–7802 (2024).
24. Guo, C., Zhang, J., Ge, Y., Qiu, Z. & Xie, Z. Asymmetric palladium migration for synthesis of chiral-at-cage *o*-carboranes. *Angew. Chem. Int. Ed.* https://doi.org/10.1002/anie.202416987 (2024).
25. Cheng, R., Zhang, J., Zhang, H., Qiu, Z. & Xie, Z. Ir-catalyzed enantioselective B–H alkenylation for asymmetric synthesis of chiral-at-cage *o*-carboranes. *Nat. Commun.* **12**, 7146 (2021).
26. Cheng, R. et al. Enantioselective Synthesis of chiral-at-cage *o*-carboranes via Pd-catalyzed asymmetric B–H substitution. *J. Am. Chem. Soc.* **140**, 4508–4511 (2018).
27. Guo, W., Guo, C., Ma, Y.-N. & Chen, X. Practical synthesis of B(9)-halogenated carboranes with *N*-haloamides in hexafluoroisopropanol. *Inorg. Chem.* **61**, 5326–5334 (2022).
28. Ma, Y.-N. et al. B(9)-OH-*o*-carboranes: synthesis, mechanism, and property exploration. *J. Am. Chem. Soc.* **145**, 7331–7342 (2023).
29. Wang, Y. et al. Highly selective electrophilic B(9)-amination of *o*-carborane driven by HOTf and HFIP. *Org. Chem. Front.* **9**, 4975–4980 (2022).
30. Wang, Y., Li, Y.-G., Chen, F., Ma, Y.-N. & Chen, X. HSAB theory guiding electrophilic substitution reactions of *o*-carborane. *Org. Chem. Front.* https://doi.org/10.1039/d4qo01546k (2024).
31. Ma, Y.-N. et al. Palladium-catalyzed regioselective B(9)-amination of *o*-carboranes and *m*-carboranes in HFIP with broad nitrogen sources. *J. Am. Chem. Soc.* **144**, 8371–8378 (2022).
32. Schnitzer, T., Budinská, A. & Wennemers, H. Organocatalysed conjugate addition reactions of aldehydes to nitroolefins with *anti* selectivity. *Nat. Catal.* **3**, 143–147 (2020).
33. Deng, T. et al. Organocatalytic asymmetric α-C–H functionalization of alkyl amines. *Nat. Catal.* **7**, 1076–1085 (2024).
34. Zhao, M. et al. Cobalt-catalyzed enantioselective reductive arylation, heteroarylation, and alkenylation of michael acceptors via an elementary mechanism of 1,4-addition. *J. Am. Chem. Soc.* **146**, 20477–20493 (2024).
35. Vastakaite, G., Budinská, A., Bögli, C. L., Boll, L. B. & Wennemers, H. Kinetic resolution of β-branched aldehydes through peptide-catalyzed conjugate addition reactions. *J. Am. Chem. Soc.* **146**, 19101–19107 (2024).
36. Chen, L. et al. Asymmetric nucleophilic additions promoted by quaternary phosphonium ion-pair catalysts. *CCS Chem.* **6**, 2110–2130 (2024).
37. Su, W. et al. Copper-catalysed asymmetric hydroboration of alkenes with 1,2-benzazaborines to access chiral naphthalene isosteres. *Nat. Chem.* **16**, 1312–1319 (2024).
38. Rossiter, B. E. & Swingle, N. M. Asymmetric conjugate addition. *Chem. Rev.* **92**, 771–806 (1992).
39. Jerphagnon, T., Pizzuti, M. G., Minnaard, A. J. & Feringa, B. L. Recent advances in enantioselective copper-catalyzed 1,4-addition. *Chem. Soc. Rev.* **38**, 1039–1075 (2009).
40. Berger, M., Ma, D., Baumgartner, Y., Wong, T. H.-F. & Melchiorre, P. Stereoselective conjugate cyanation of enals by combining photoredox and organocatalysis. *Nat. Catal.* **6**, 332–338 (2023).
41. Schnurr, M., Rackl, J. W. & Wennemers, H. Overcoming deactivation of amine-based catalysts: access to fluoroalkylated γ-nitroaldehydes. *J. Am. Chem. Soc.* **145**, 23275–23280 (2023).
42. Suzuki, H., Moro, R. & Matsuda, T. Palladium-catalyzed *anti*-Michael-type (Hetero)arylation of acrylamides. *J. Am. Chem. Soc.* **146**, 13697–13702 (2024).
43. Kang, G., Strassfeld, D. A., Sheng, T., Chen, C.-Y. & Yu, J.-Q. Transannular C–H functionalization of cycloalkane carboxylic acids. *Nature* **618**, 519–525 (2023).
44. Zhang, T. et al. Enantioselective remote methylene C–H (hetero) arylation of cycloalkane carboxylic acids. *Science* **384**, 793–798 (2024).
45. Wang, T.-C. et al. Stereoselective amino acid synthesis by photobiocatalytic oxidative coupling. *Nature* **629**, 98–104 (2024).
46. Ren, H. et al. Direct B–H functionalization of icosahedral carboranes via hydrogen atom transfer. *J. Am. Chem. Soc.* **145**, 7638–7647 (2023).
47. Zhang, Q., Wu, L.-S. & Shi, B.-F. Forging C–heteroatom bonds by transition-metal-catalyzed enantioselective C–H functionalization. *Chem.* **8**, 384–413 (2022).
48. Zhang, Q. & Shi, B.-F. 2-(Pyridin-2-yl)isopropyl (PIP) amine: an enabling directing group for divergent and asymmetric functionalization of unactivated methylene C($sp^3$)-H bonds. *Acc. Chem. Res.* **54**, 2750–2763 (2021).
49. Wakchaure, V. N. et al. Catalytic asymmetric cationic shifts of aliphatic hydrocarbons. *Nature* **625**, 287–292 (2024).
50. Wagen, C. C., McMinn, S. E., Kwan, E. E. & Jacobsen, E. N. Screening for generality in asymmetric catalysis. *Nature* **610**, 680–686 (2022).
51. Singh, V. K. et al. Taming secondary benzylic cations in catalytic asymmetric $S_N1$ reactions. *Science* **382**, 325–329 (2023).
52. Dziedzic, R. M. et al. Cage-walking: vertex differentiation by palladium-catalyzed isomerization of B(9)-bromo-*meta*-carborane. *J. Am. Chem. Soc.* **139**, 7729–7732 (2017).
53. Frisch, M. J. et al. Gaussian 16, Revision B.01 (Gaussian Inc., 2016).
54. Gao, T. et al. Stereodivergent synthesis through catalytic asymmetric reversed hydroboration. *J. Am. Chem. Soc.* **141**, 4670–4677 (2019).
55. Bader, R. F. W. A quantum theory of molecular structure and its applications. *Chem. Rev.* **91**, 893–928 (1991).
56. Zhang, X. et al. B–H···π interaction: a new type of nonclassical hydrogen bonding. *J. Am. Chem. Soc.* **138**, 4334–4337 (2016).


## Acknowledgements

This work was supported by National Natural Science Foundation of China (grant nos. 22271256 to Y.-N.M.; U23A2078 and 22171246 to X.C.; 22473100 to D.W.), Natural Science Foundation of Henan Province (grant nos. 232301420046 and 232300421088 to Y.-N.M.) and the Key Project of the Joint Fund for Science and Technology Research and Development in Henan Province (grant no. 232301420008 to D.W.).

## Author contributions

Y.-N.M. and X.C. conceived and designed the study. D.W. directed the DFT calculations and mechanism analysis. C.L. and W.L. conducted most experiments on the asymmetric reactions. T.S. conducted the DFT calculations. Y.-X.W. conducted the experiments on the synthesis of ligands. M.H. conducted the experiments on the synthesis of substrates. Y.-N.M. and X.C. prepared the manuscript. C.L. prepared the Supplementary Information.

## Competing interests

The authors declare no competing interests.

## Additional information

**Supplementary information** The online version contains supplementary material available at https://doi.org/10.1038/s41929-026-01480-4.

**Correspondence and requests for materials** should be addressed to Donghui Wei, Yan-Na Ma or Xuenian Chen.

**Peer review information** *Nature Catalysis* thanks the anonymous reviewer(s) for their contribution to the peer review of this work.